

Soft and Stiff Normal Modes in Floppy Colloidal Square Lattices

Julio Melio¹, Silke E. Henkes², and Daniela J. Kraft^{1,*}

¹*Huygens-Kamerlingh Onnes Laboratory, Leiden University, P.O. Box 9504, 2300 RA Leiden, The Netherlands*

²*Lorentz Institute, Leiden University, P.O. Box 9506, 2300 RA Leiden, The Netherlands*

 (Received 24 July 2023; revised 8 November 2023; accepted 3 January 2024; published 14 February 2024)

Floppy microscale spring networks are widely studied in theory and simulations, but no well-controlled experimental system currently exists. Here, we show that square lattices consisting of colloid-supported lipid bilayers functionalized with DNA linkers act as microscale floppy spring networks. We extract their normal modes by inverting the particle displacement correlation matrix, showing the emergence of a spectrum of soft modes with low effective stiffness in addition to stiff modes that derive from linker interactions. Evaluation of the softest mode, a uniform shear mode, reveals that shear stiffness decreases with lattice size. Experiments match well with Brownian particle simulations, and we develop a theoretical description based on mapping interactions onto a linear response model to describe the modes. Our results reveal the importance of entropic steric effects and can be used for developing reconfigurable materials at the colloidal length scale.

DOI: [10.1103/PhysRevLett.132.078202](https://doi.org/10.1103/PhysRevLett.132.078202)

Networks below the mechanical stability threshold exhibit large-scale, low-energy deformation modes [1]. These floppy modes play an important role in a wide range of systems, ranging from elastic networks [2,3] to particle packings [4], and are also important for understanding the rheological behavior of colloidal gels [5] and biopolymer networks [6], the glass transition in disordered solids [7], and protein flexibility [8]. Floppy modes in frictionless ordered [1] and disordered [2,9] packings and networks have been shown to be strictly zero-energy deformations. In contrast, floppy modes in microscale networks have been predicted by simulations and theoretical arguments to be stabilized by thermal fluctuations, resulting in nonzero shear moduli even below the isostatic point [10–13], and they are expected to possess an anomalous temperature dependence of the shear modulus [10,11].

While bonded colloidal structures that can rearrange have been experimentally realized using patchy particles [14] and colloids coated with surface-bound DNA linkers which can roll over each other's surfaces close to the melting temperature [15,16], neither allows for a fixed bond network topology, and they are thus limited to structures accessible by free energy minimization. An experimental model system that combines full flexibility with a fixed bond network topology and springlike bonds is currently missing, yet it would allow testing of these predictions and

lead to a better understanding of thermally excited floppy modes. In addition, it would enable the translation of concepts developed in mechanical metamaterials to the microscale, where floppy modes are exploited to obtain specifically engineered capabilities such as shape morphing [17] or topology-dependent mechanical properties [18].

Here, we present an experimental system that behaves as a floppy microscale spring network and allows *in situ* observation of the dynamics and thermal excitations by optical microscopy. We build two-dimensional colloidal square lattices and find that they display soft shear modes with a small but finite stiffness 2–3 orders of magnitude softer than the stiffer compression modes, which is different from disordered [5] or large crystalline [19,20] systems. The extracted modes show good agreement with Brownian particle simulations and a theoretical mapping onto a linear response model.

Creating experimental floppy colloidal square lattices.—To create floppy square lattices, we employ colloid-supported lipid bilayers (CSLBs) functionalized with two complementary strands of DNA linkers, as shown in Fig. 1(a) and described in Verweij *et al.* [21] and in Sec. I of the Supplemental Material [22] in more detail. At room temperature, the linkers provide selective, irreversible binding, while inert DNA strands and PEGylated lipids provide steric stabilization. The DNA can freely move within the fluid bilayer, unaffected by the individual particle rotation, which allows the particles to fully reconfigure with respect to each other while remaining bound. We assemble 2.12 ± 0.06 μm diameter particles one by one into square lattices of size $n \times n$ with $n = 2, 3, 4, 5, 7$ using optical tweezers. This is an easily scalable floppy system, as it is isostatic in the infinite limit using simple constraint

Published by the American Physical Society under the terms of the [Creative Commons Attribution 4.0 International license](https://creativecommons.org/licenses/by/4.0/). Further distribution of this work must maintain attribution to the author(s) and the published article's title, journal citation, and DOI.

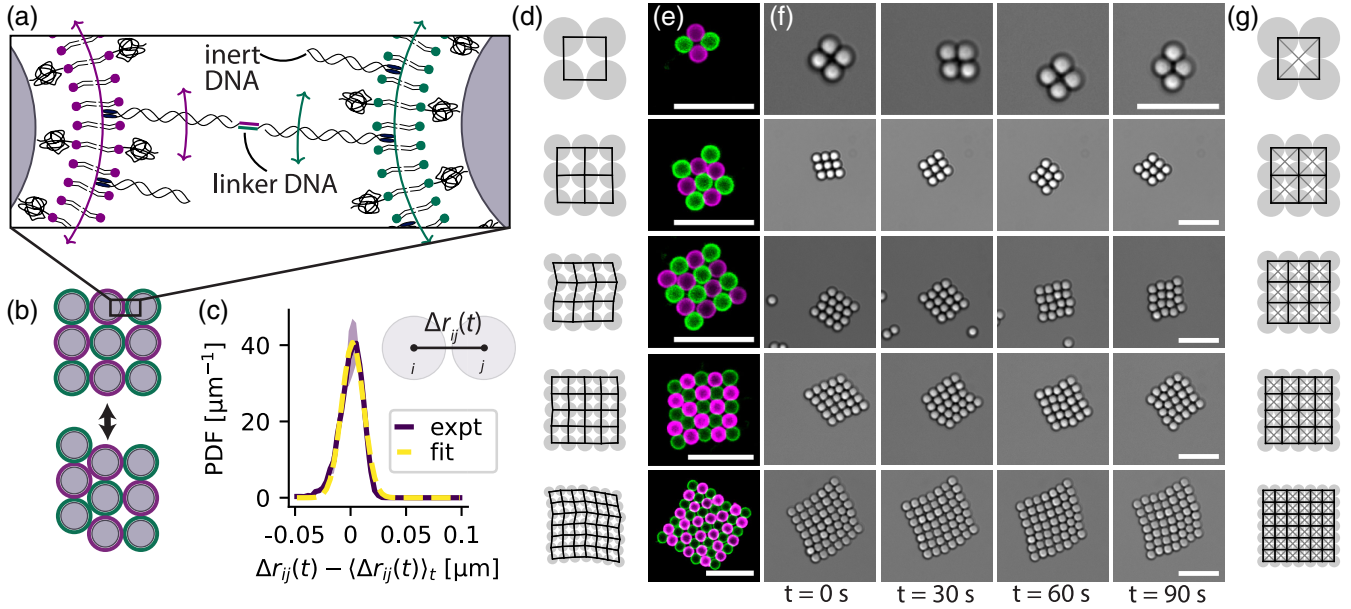


FIG. 1. *Flexible colloidal square lattices.* (a) A schematic overview of the binding mechanism. Silica particles are coated with a fluid lipid bilayer functionalized with linker double-stranded (ds) DNA with single-stranded sticky ends that enable strong and specific binding yet are laterally mobile, thereby providing the ability for rearrangements after binding. Colloidal stability is provided by PEGylated lipids and inert dsDNA. (b) A schematic example of a floppy mode deformation in a 3×3 square lattice. (c) The distribution of the distance between two particles i and j , $\Delta r_{ij}(t) - \langle \Delta r_{ij} \rangle_t$, measured on particle pairs can be well approximated with a normal distribution yielding a bond stiffness of $k_{\text{bond}} = 43 \pm 1 \mu\text{Nm}^{-1}$. (d) Time-averaged particle positions as measured in experiments, where the bond network is indicated in black. (e) Confocal images of the $n \times n$ square lattices with $n = 2, 3, 4, 5, 7$, where the color indicates functionalization with different, complementary DNA linkers. (f) Brightfield snapshots of the same lattices taken 30 s apart. (g) Spring networks used in the theoretical description, with the particle bonds indicated in black and the effective diagonal interactions indicated in gray. Scale bars are 10 μm .

counting [26], but it admits $2n - 3$ floppy modes that correspond to shear deformations between layers when cut to a finite size [1] (see also Sec. III A of the Supplemental Material [22]). An example of such a floppy mode displacement for a 3×3 lattice is schematically shown in Fig. 1(b). Once assembled from complementary CSLBs marked with different fluorescent lipids [see Fig. 1(e)], the square lattice structure cannot change its network topology, because bonds between particles diagonally opposite of each other are not possible by design.

We observe the dynamics of the assembled lattices with a brightfield microscope at a frame rate of 20 fps. The particles move predominantly in 2D (with a gravitational height of 53 nm) and are freely jointed to very good approximation [21,27]. Because of their size, the thus assembled lattices undergo thermal motion in the form of translation and rotation, but also by changing their conformations, which is evident from the snapshots taken 30 s apart shown in Fig. 1(f) and in Movies 1–5 of the Supplemental Material, where the thermally excited shear modes are clearly visible.

We start by showing that the multivalent DNA bonds between the CSLBs can be approximated by harmonic springs. To do so, we quantify the particle positions of a pair of particles from brightfield microscopy videos

using a tracking method with subpixel accuracy named HoloPy [21,28]. This allows for detecting variations on the order of nanometers, so not only are the floppy modes tracked with high accuracy, but also elastic normal modes that happen on the scale of several tens of nanometers. We plot the bond length variation $\Delta r_{ij} - \langle \Delta r_{ij} \rangle_t$ in Fig. 1(c), where Δr_{ij} is the distance between the centers of particles i and j , and $\langle \dots \rangle_t$ denotes an average over the measurement time. A Gaussian fit with spring constant $k_{\text{bond}} = 43 \pm 1 \mu\text{Nm}^{-1}$ agrees well with the experimental data. The multivalent patch of DNA linkers therefore acts as a spring, implying that CSLB-based colloidal structures are effectively microscale spring networks, at least to lowest order. The springlike bond networks are schematically drawn in Fig. 1(d).

Results and interpretation.—We analyze the particle trajectories [see Fig. 2(a)] to obtain the vibrational modes for a 2×2 lattice with $N = n^2 = 4$ particles and $2N = 8$ degrees of freedom. We subtract the motion due to the three trivial translational and rotational degrees of freedom to obtain the trajectories shown in Fig. 2(b) (see Sec. IC of the Supplemental Material [22] for details). As expected, particles move predominantly on the diagonals, corresponding to the shearlike motion observed in experiments.

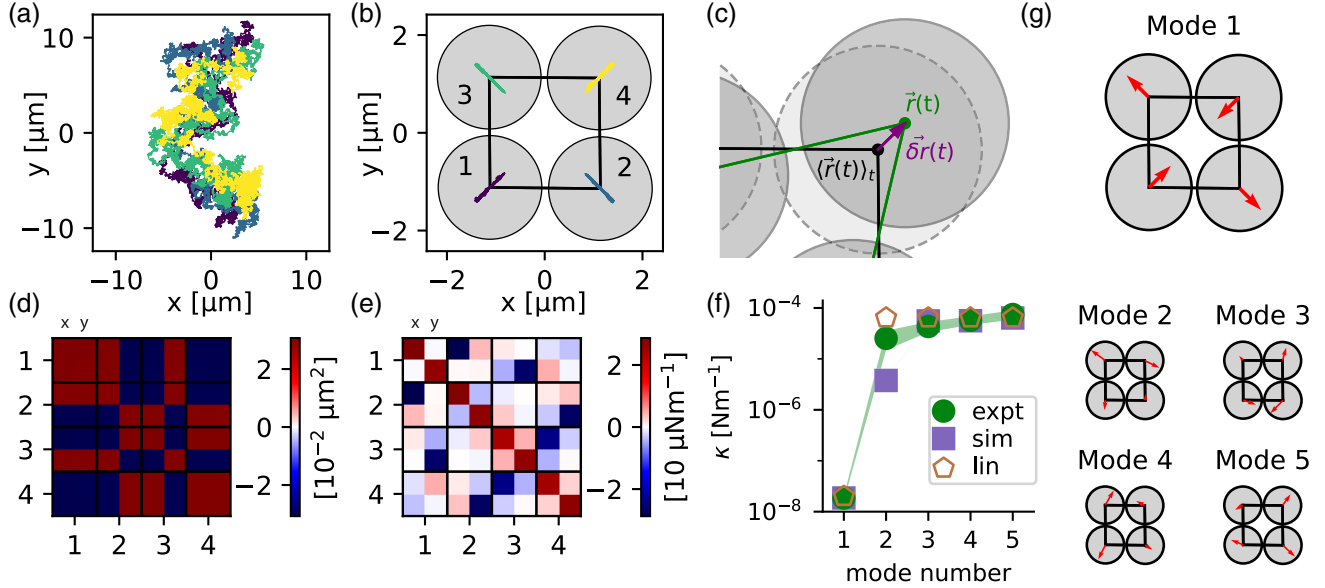


FIG. 2. *Mode calculation for a 2×2 structure.* (a) Typical trajectories for a 2×2 lattice, where the different colors represent the four different particles. (b) The same trajectories after subtracting translation and rotation, where the average position over time $\langle \vec{r}(t) \rangle_t$ is shown and the particles are labeled. (c) A schematic showing the equilibrium position $\langle \vec{r}(t) \rangle_t$, the position at time t , $\vec{r}(t)$, and the displacement vector $\delta \vec{r}(t)$. (d) Experimentally measured covariance matrix of the displacement vectors C_p , which is pseudoinverted to obtain (e) the stiffness matrix \mathbf{K} . (f) The eigenvalues of \mathbf{K} representing the mode stiffnesses κ for experiments (expt), Brownian particle simulations (sim) with $k_{\text{bond}} = 32 \mu\text{Nm}^{-1}$, and a map onto linear response (lin) with $k_{\text{bond}} = 32 \mu\text{Nm}^{-1}$ and $k_{\text{diag}} = 10 \text{nNm}^{-1}$. (g) The experimentally obtained eigenvectors of \mathbf{K} represent the vibrational modes.

For colloidal glasses [29–31] and crystals [19,20], which do not have floppy modes, equilibrium fluctuation-dissipation relations have been exploited to link particle fluctuations to stiffnesses in the dynamical matrix, in a spirit similar to passive microrheology [32]. We use this fluctuation-inversion method based on equipartition in the form developed by one of us [33] to obtain the stiffness matrix \mathbf{K} . Briefly, we compute the $2N$ particle displacement vector $\delta \vec{r}(t) = \vec{r}(t) - \langle \vec{r}(t) \rangle_t$, where $\langle \dots \rangle_t$ denotes a time average over the experiment [see Fig. 2(c)]. From this, the $2N \times 2N$ covariance matrix of the displacements, $C_p = \langle \delta \vec{r}(t) \cdot \delta \vec{r}(t) \rangle$, is calculated [see Fig. 2(d)]. In the long-time limit and in linear response, the stiffness matrix \mathbf{K} is related to C_p by $\mathbf{K} = k_B T C_p^{-1}$ [33] [see Fig. 2(e)], where we now need to use the pseudoinverse, because C_p is singular [34] as a result of subtracting the trivial modes. The eigenvectors of C_p and \mathbf{K} represent the normal modes, and the eigenvalues of \mathbf{K} , κ , represent the mode stiffnesses. C_p only contains two distinctive values, matching the earlier observation that particles move on diagonals. In \mathbf{K} , in addition to the diagonal terms that indicate confinement, we observe large stiffness values along the pair bond directions, as well as smaller values that indicate next-nearest-neighbor (NNN) interactions.

The $2N - 3 = 5$ mode stiffnesses κ are shown in Fig. 2(f) with increasing stiffness. For the experimental data, a $\sim 10^3$ difference in stiffness is visible between the

softest mode and the stiffer modes. The modes themselves, obtained from the eigenvectors of \mathbf{K} , are plotted in Fig. 2(g). The softest mode is the expected shear mode that involves no changes in bond lengths and thus is a floppy mode. The other four normal modes are significantly stiffer, as bonds have to be compressed or extended.

Theoretical description.—To better understand the experimental results and test if all relevant interactions are taken into account, we perform Brownian particle simulations (see Sec. II of the Supplemental Material [22]). In these simulations, particle neighbors are fixed and connected by springs of stiffness $k_{\text{bond}} = 32 \mu\text{Nm}^{-1}$. We solve the overdamped Langevin equation in two dimensions with explicit thermal noise and friction. The correct topology is assured by an additional one-sided, repulsive spring of stiffness k_{bond} that only becomes active when two particles overlap that are not neighbors. The resulting soft mode stiffness is in excellent agreement with the experimental result, and the stiffer modes 3–5 match experiments very well, but we find a noticeably lower value for mode 2 [see the data point labeled “sim” in Fig. 2(f), and Fig. S4 in the Supplemental Material]. Differences between experiments and simulations might stem from variations in the spring constants arising from varying DNA concentrations between particles [35] and consecutive binding of colloids, small 3D movement causing the springs to appear softer, imperfections of the colloids, or

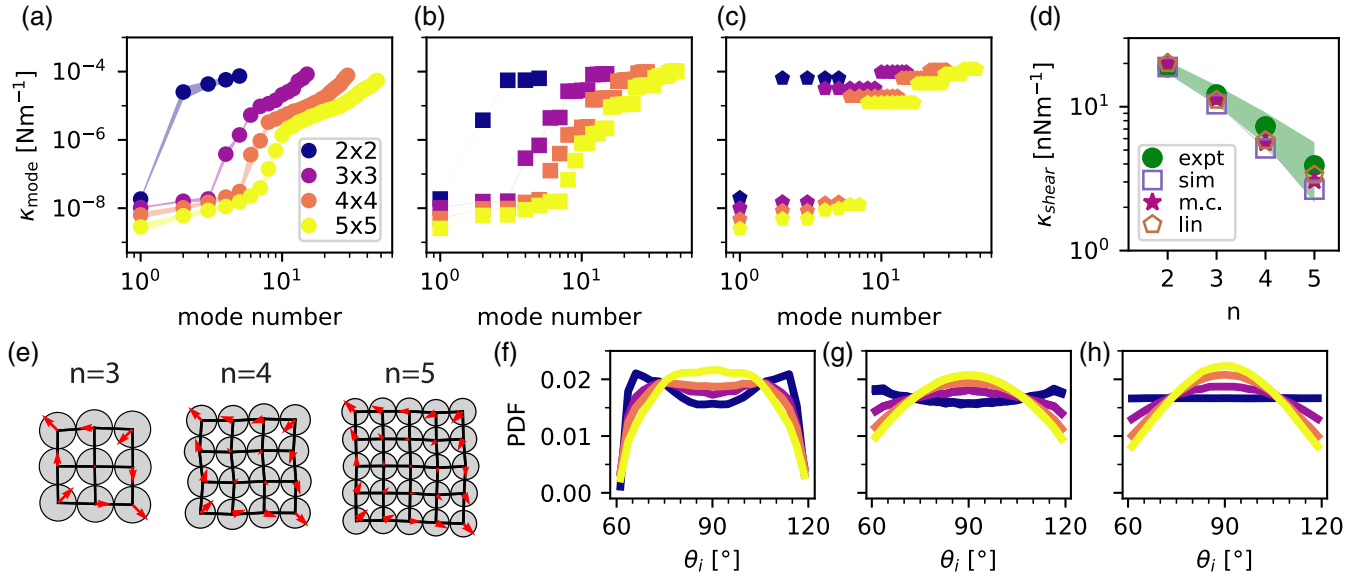


FIG. 3. *Modes for larger systems.* (a)–(c): The mode stiffnesses of larger lattices $n \times n$ for (a) experiments (expt), (b) simulations (sim), and (c) a theoretical map onto linear response (lin), where the line width is equivalent to the standard deviation. (d) The shear stiffness obtained from the variance of the shear mode projection distribution as a function of n , where the experimental standard deviation is indicated, and the Monte Carlo approach is denoted by “m.c.” (e) Schematics of the softest mode, which is close to a pure shear mode. (f)–(h): The opening angle distributions for (f) experiments, (g) simulations, and (h) the Monte Carlo approach. Simulations and linear response results are obtained using $k_{\text{bond}} = 32 \mu\text{Nm}^{-1}$ and the k_{diag}^n derived below. For the linear response data, $\kappa_{\text{shear}}^{\text{lin}} = (\sum_{\nu} (1/\kappa_{\nu})(\vec{m} \cdot \vec{\xi}_{\nu})^2)^{-1}$ with $\vec{\xi}_{\nu}$ the eigenvector of \mathbf{K} for mode ν is plotted in panel (d).

tracking errors (see Sec. V of the Supplemental Material [22] for a discussion).

We now map these results to a linear response model where we assume fixed bond lengths and a uniform opening angle distribution to get an effective diagonal bond with a stiffness of $k_{\text{diag}} = \frac{1}{2}(2/d^2)[k_{\text{B}}T/\text{Var}(\theta)] = (108k_{\text{B}}T/\pi^2d^2)$ (see Sec. III B of the Supplemental Material [22]), where the factor $\frac{1}{2}$ comes from dividing the spring over two diagonals. For $d = 2.12 \mu\text{m}$ and above assumptions, $k_{\text{diag}} = 10 \text{ nNm}^{-1}$. The resulting spring networks are indicated in Fig. 1(g). We can then obtain the modes and their stiffnesses by diagonalizing the constructed stiffness matrix (see Sec. III C of the Supplemental Material [22]) with neighbor stiffness k_{bond} and NNN diagonal effective stiffness k_{diag} . A similar approach was employed by Ref. [14] to derive effective angle springs and low-energy modes in a Kagome lattice. We obtain three modes with a stiffness of $2k_{\text{bond}}$, one with a stiffness of $2(k_{\text{bond}} + k_{\text{diag}})$, and one with stiffness $2k_{\text{diag}}$ [labeled with “lin” in Fig. 2(f)]. The stiffness of the soft mode, 20.0 nNm^{-1} , is very similar to experiments and simulations, both with 19.2 nNm^{-1} , while the stiff modes are of the same order of magnitude. Comparison between linear response and simulations reveals that the stiff modes acquire a nonlinear component due to the large deformations. The most notable difference for compression mode 2 can be matched to a projection of the floppy mode onto this

mode. In experiments, this effect is nearly fully counteracted by an experimentally observed angle-bond length correlation (see Sec. V of the Supplemental Material [22]).

Larger square lattices.—Having obtained a comprehensive understanding of the 2×2 structure, we now turn to larger square lattices with more soft modes. In Figs. 3(a)–3(c), the mode stiffnesses are shown as a function of mode number for experiments, Brownian particle simulations, and the linear response approach discussed below, respectively. For our finite systems, Maxwell constraint counting [26] corresponds to $2n^2$ translational degrees of freedom that are countered by $2n^2 - 2n$ bonds, giving us $2n - 3$ floppy modes after taking into account global degrees of freedom (see also Sec. III A of the Supplemental Material). We indeed find 1, 3, 5, and 7 soft modes for 2×2 , 3×3 , 4×4 , and 5×5 experimental square lattices, respectively. Similarly to the results for the 2×2 structure, we find very good agreement for the stiffness of the floppy modes, while the stiffer modes are of the same order of magnitude, and the simulations show groups of near degenerate modes not apparent in experiments.

The softest modes, shown in Fig. 3(e), are nearly pure shear modes. We compute a shear modulus by projecting the experimental trajectories onto a normalized pure shear mode: \vec{m} : $p(t) = \delta\vec{r}(t) \cdot \vec{m}$. The distributions $P_n(p)$ for experiments and simulations become more Gaussian with increasing system size, as is visible in Fig. S7 in the

Supplemental Material. Using equipartition, we can compute the stiffness of the shear mode $\kappa_{\text{shear}} = k_B T / \text{Var}(p)$ [see Fig. 3(d)]. Clearly, the shear modulus decreases with system size. The diffusion of the lattices does not couple to this shear mode excitation (see Fig. S8 in the Supplemental Material).

We can understand its origin and derive its value as follows: each angle has a range between $(\pi/3)$ and $(2\pi/3)$, but due to entropic effects stemming from the geometric constraints imposed by the square lattice topology, the angle distribution for larger systems narrows [see Fig. 3(f)], similarly to what we have previously observed for flexible colloidal rings [21]. This means that entropic effects effectively stabilize the open structure, in line with predictions [10,13] and experiments on patchy particles [14]. Using a Monte Carlo approach where we assume fixed bond lengths and only select sterically allowed angle combinations (see Sec. IV in the Supplemental Material [22]), we find angle distributions $P(\theta_{nxn})$ that closely match experiments and simulations, as shown in Figs. 3(f)–3(h). This corroborates the entropic origin of the narrowing of the angle distribution. Moreover, using this approach, we are able to correctly predict the shear mode distribution $P_n(p)$ (see Fig. S7 in the Supplemental Material) and the shear modulus [see the “m.c.” symbols in Fig. 3(d)].

To map to linear response, we again introduce NNN springs that derive from the steric constraints, but we need to modify our argument: While there are $(n-1)^2$ floppy squares in the packing, there are only $2n-3$ independent opening angles in the stiff bond limit. To take this effect and the angle distributions into account, we calculate the diagonal spring interaction k_{diag}^n for larger systems by scaling k_{diag} as $k_{\text{diag}}^n = [(2n-3)/(n-1)^2][\text{Var}(\theta_{2x2})/\text{Var}(\theta_{nxn})]k_{\text{diag}}$. We show the resulting mode spectrum in Fig. 3(c). The soft modes are well described by linear response, and the stiff modes are on the right order of magnitude. Furthermore, the nondegeneracy of the stiffer modes in simulations indicates the presence of higher-order, nonlinear effects due to large lattice deformations, which are also visible in experiments. See Sec. V of the Supplemental Material [22] for a more extensive discussion.

To summarize, our experimental model system provides a way to make microscale spring networks with a fixed bond network topology, a linear response model well describes the soft modes and linear part of the stiff modes, and we find a modified scaling of the shear modulus with system size due to entropic effects as predicted [10–13].

Our understanding of floppy colloidal networks can serve as a starting point for studying thermal effects in more complex network topologies, as well as designing and analyzing colloidal structures with global reconfiguration modes with more advanced functionalities, such as colloidal mechanical metamaterials or self-assembled adaptive materials.

D.J.K. gratefully acknowledges funding from the European Research Council (ERC) under the European Union’s Horizon 2020 research and innovation program (Grant Agreement No. 758383). S.H. acknowledges lively discussions with Fred MacKintosh and the hospitality of the Isaac Newton Institute for Mathematical Sciences during the SPL program, supported by EPSRC Grant No. EP/R014604/1.

*Corresponding author: kraft@physics.leidenuniv.nl

- [1] T. C. Lubensky, C. L. Kane, X. Mao, A. Souslov, and K. Sun, Phonons and elasticity in critically coordinated lattices, *Rep. Prog. Phys.* **78**, 073901 (2015).
- [2] W. G. Ellenbroek, V. F. Hagh, A. Kumar, M. F. Thorpe, and M. van Hecke, Rigidity loss in disordered systems: Three scenarios, *Phys. Rev. Lett.* **114**, 135501 (2015).
- [3] S. Chen, F. Giardina, G. P. Choi, and L. Mahadevan, Modular representation and control of floppy networks, *Proc. R. Soc. A* **478**, 2022.0082 (2022).
- [4] A. J. Liu and S. R. Nagel, The jamming transition and the marginally jammed solid, *Annu. Rev. Condens. Matter Phys.* **1**, 347 (2010).
- [5] D. Z. Rocklin, L. Hsiao, M. Szakasits, M. J. Solomon, and X. Mao, Elasticity of colloidal gels: Structural heterogeneity, floppy modes, and rigidity, *Soft Matter* **17**, 6929 (2021).
- [6] C. Broedersz and F. MacKintosh, Modeling semiflexible polymer networks, *Rev. Mod. Phys.* **86**, 995 (2014).
- [7] A. Widmer-Cooper, H. Perry, P. Harrowell, and D. R. Reichman, Irreversible reorganization in a supercooled liquid originates from localized soft modes, *Nat. Phys.* **4**, 711 (2008).
- [8] L. Meireles, M. Gur, A. Bakan, and I. Bahar, Pre-existing soft modes of motion uniquely defined by native contact topology facilitate ligand binding to proteins, *Protein Sci.* **20**, 1645 (2011).
- [9] M. van Hecke, Jamming of soft particles: Geometry, mechanics, scaling and isostaticity, *J. Phys. Condens. Matter* **22**, 033101 (2009).
- [10] M. Dennison, M. Sheinman, C. Storm, and F. C. MacKintosh, Fluctuation-stabilized marginal networks and anomalous entropic elasticity, *Phys. Rev. Lett.* **111**, 095503 (2013).
- [11] X. Mao, A. Souslov, C. I. Mendoza, and T. C. Lubensky, Mechanical instability at finite temperature, *Nat. Commun.* **6**, 5968 (2015).
- [12] L. Zhang and X. Mao, Finite-temperature mechanical instability in disordered lattices, *Phys. Rev. E* **93**, 022110 (2016).
- [13] H. Hu, P. S. Ruiz, and R. Ni, Entropy stabilizes floppy crystals of mobile DNA-coated colloids, *Phys. Rev. Lett.* **120**, 048003 (2018).
- [14] X. Mao, Q. Chen, and S. Granick, Entropy favours open colloidal lattices, *Nat. Mater.* **11**, 217 (2013).
- [15] Y. Wang, Y. Wang, X. Zheng, E. Ducrot, J. S. Yodh, M. Weck, and D. J. Pine, Crystallization of DNA-coated colloids, *Nat. Commun.* **6**, 7253 (2015).

- [16] H. Fang, M.F. Hagan, and W.B. Rogers, Two-step crystallization and solid-solid transitions in binary colloidal mixtures, *Proc. Natl. Acad. Sci. U.S.A.* **117**, 27927 (2020).
- [17] C. Coulais, E. Teomy, K. De Reus, Y. Shokef, and M. Van Hecke, Combinatorial design of textured mechanical metamaterials, *Nature (London)* **535**, 529 (2016).
- [18] H. Xiu, H. Liu, A. Poli, G. Wan, K. Sun, E. M. Arruda, X. Mao, and Z. Chen, Topological transformability and reprogrammability of multistable mechanical metamaterials, *Proc. Natl. Acad. Sci. U.S.A.* **119**, e2211725119 (2022).
- [19] P. Keim, G. Maret, U. Herz, and H.H. von Grünberg, Harmonic lattice behavior of two-dimensional colloidal crystals, *Phys. Rev. Lett.* **92**, 215504 (2004).
- [20] K. Chen, T. Still, S. Schoenholz, K. B. Aptowicz, M. Schindler, A. C. Maggs, A. J. Liu, and A. G. Yodh, Phonons in two-dimensional soft colloidal crystals, *Phys. Rev. E* **88**, 022315 (2013).
- [21] R. W. Verweij, J. Melio, I. Chakraborty, and D. J. Kraft, Brownian motion of flexibly-linked colloidal rings, *Phys. Rev. E* **107**, 034602 (2023).
- [22] See Supplemental Material at <http://link.aps.org/supplemental/10.1103/PhysRevLett.132.078202> for details on experiments, simulations, the theoretical model, and the Monte Carlo approach, as well as a quantitative comparison of the stiff modes, the shear mode projection distribution, and diffusion constants, which additionally includes Refs. [23–25].
- [23] C. Linne, D. Visco, S. Angioletti-Uberti, L. Laan, and D. J. Kraft, Direct visualization of superselective colloid-surface binding mediated by multivalent interactions, *Proc. Natl. Acad. Sci. U.S.A.* **118**, e2106036118 (2021).
- [24] M. Rinaldin, R. W. Verweij, I. Chakraborty, and D. J. Kraft, Colloid supported lipid bilayers for self-assembly, *R. Soc. Chem.* **15**, 1345 (2019).
- [25] C. van der Wel and D. J. Kraft, Automated tracking of colloidal clusters with sub-pixel accuracy and precision, *J. Phys. Condens. Matter* **29**, 044001 (2017).
- [26] J. C. Maxwell, On the calculation of the equilibrium and stiffness of frames, *London Edinburgh Dublin Phil. Mag. J. Sci.* **27**, 294 (1864).
- [27] R. W. Verweij, P. G. Moerman, L. P. Huijnen, N. E. Ligthart, I. Chakraborty, J. Groenewold, W. K. Kegel, A. van Blaaderen, and D. J. Kraft, Conformations and diffusion of flexibly linked colloidal chains, *J. Phys.* **4**, 035002 (2021).
- [28] S. Barkley, T. G. Dimiduk, J. Fung, D. M. Kaz, V. N. Manoharan, R. McGorty, R. W. Perry, and A. Wang, Holographic microscopy with PYTHON and HOLOPY, *Comput. Sci. Eng.* **22**, 72 (2020).
- [29] K. Chen, W. G. Ellenbroek, Z. Zhang, D. T. N. Chen, P. J. Yunker, S. Henkes, C. Brito, O. Dauchot, W. Van Saarloos, A. J. Liu, and Y. A. G., Low-frequency vibrations of soft colloidal glasses, *Phys. Rev. Lett.* **105**, 025501 (2010).
- [30] D. Kaya, N. L. Green, C. E. Maloney, and M. F. Islam, Normal modes and density of states of disordered colloidal solids, *Science* **329**, 656 (2010).
- [31] A. Ghosh, V. K. Chikkadi, P. Schall, J. Kurchan, and D. Bonn, Density of states of colloidal glasses, *Phys. Rev. Lett.* **104**, 248305 (2010).
- [32] D. Mizuno, D. Head, F. MacKintosh, and C. Schmidt, Active and passive microrheology in equilibrium and non-equilibrium systems, *Macromolecules* **41**, 7194 (2008).
- [33] S. Henkes, C. Brito, and O. Dauchot, Extracting vibrational modes from fluctuations: A pedagogical discussion, *Soft Matter* **8**, 6092 (2012).
- [34] R. Penrose and J. A. Todd, On best approximate solutions of linear matrix equations, *Math. Proc. Cambridge Philos. Soc.* **52**, 17 (1956).
- [35] I. Chakraborty, V. Meester, C. Van Der Wel, and D. J. Kraft, Colloidal joints with designed motion range and tunable joint flexibility, *Nanoscale* **9**, 7814 (2017).